Tether-Based Localization for Cooperative Ground and Aerial Vehicles

Andrea Borgese, Dario C. Guastella, *Member, IEEE*, Giuseppe Sutera, and Giovanni Muscato, *Senior Member, IEEE*

***Abstract*—Considering a multi-robot system composed of a ground vehicle and a multi-copter connected each other with a tether, it is crucial for them to know their relative positions in order to carry out any operating task. Localization is usually accomplished by using GPS in outdoor environments. However, such a system does not work in indoor and more generally in so-called GPS denied environments. We investigated a solution which exploits the catenary configuration assumed by tether and does not require any computationally demanding resource or complex cable tension sensors. Different approaches have been experimentally tested, compared and validated with classical localization systems in both indoor and outdoor environments.**

***Index Terms*—Aerial systems: applications, localization, multi-robot systems.**

I. Introduction

UNMANNED aerial vehicles (UAVs) are widely used in different scenarios, including search and rescue [1], [2], post-disaster monitoring [3], and chemical, biological, radiological and nuclear risk (CBRN) management [4], [5]. In particular, multi-rotors have been employed in an increasing number of solutions, thanks to their capability to hover and to vertically take off and land which makes them particularly suitable for aerial inspections and reconnaissance.

However, the time available for multi-copters to carry out a mission represents a relevant limit, since the maximum flight time of these vehicles is typically below 20 minutes. The adoption of tethering systems has recently been proposed in the literature to provide the drone with a continuous power supply [6], [7], thus increasing the flight time. Furthermore, the presence of a cable allows the recovery of the UAV in case of failure or loss of control [8]. However, fixed tethering systems constrain the UAV operating space. To overcome this issue, the adoption of a *heterogeneous* team of *tethered* vehicles has recently been proposed to take advantage of the complementary features and strengths provided by the different types of platforms [9]–[12]. For instance, in the case of missions for visual inspections, an aerial vehicle provides a better perspective, compared to a ground platform, which has a higher payload and allows the transportation of long-autonomy batteries.

In this context, the relative localization of the two tethered vehicles represents a crucial problem for the correct navigation and coordination of the robotic team. The aim of this letter is to propose a localization technique between an Unmanned Ground Vehicle (UGV) and a multi-rotor that are connected each other with a slack tether. This solution is grounded on the idea that the tether shapes as a catenary curve while the aerial vehicle is hovering during a mission. Few solutions are present in the literature exploiting this idea. The main novelty of our localization approach compared to such solutions lies in the possibility to estimate the relative position and the heading of the aerial vehicle with respect to the field robot by proposing a low-cost, computationally light sensing of the tether direction angles. In particular, such angles are sensed at both ends of the cable, as opposed to current solutions available in the literature, which improves the localization performance without the need to adopt any sensor for the cable tension.

The main contributions of this letter are:

- the proposed sensing solution of the tether direction angles at the two ends
- the investigation of sensors' mechanical design and implementation
- the experimental analysis performed in both indoor and outdoor environments, including a comparison with commonly adopted localization solutions for both scenarios

II. Related Work

When dealing with outdoor areas, localization solutions typically rely on GPS (Global Positioning System) data. To increase the positioning accuracy, up to the order of a centimeter, the RTK (Real-Time Kinematic) technology can be adopted, which, however, requires an additional device placed in a point of known coordinates, acting as a base, or a connection to a so-called NTRIP server. However, there are many scenarios where such an approach is severely negatively affected by so-called multi-path effect and shadowing (e.g., urban canyon problem) or cannot be used at all (e.g., in indoor environments).

Manuscript received 24 February 2022; accepted 21 June 2022. Date of publication 30 June 2022; date of current version 7 July 2022. This letter was recommended for publication by Associate Editor S. L. Waslander and Editor J. Civera upon evaluation of the reviewers' comments. This work was supported by Safe and Smart Farming with Artificial Intelligence and Robotics (S2-FAIR), Agriculture, Green and Digital (AGREED) and PNR 2015-2020 PON Ricerca e Innovazione REACT-EU "Metodologie e tecnologie innovative per la robotica manipolativa, mobile, collaborativa per l'industria 4.0". *A. Borgese, D. C. Guastella, and G. Sutera contributed equally to this work. (Corresponding author: Dario C. Guastella.)*

The authors are with the Dipartimento di Ingegneria Elettrica Elettronica e Informatica, Università degli Studi di Catania, 95124 Catania, Italy (e-mail: andrea.borgese@phd.unict.it; dario.guastella@dieei.unict.it; giuseppe.sutera@unict.it; giovanni.muscato@unict.it).

Digital Object Identifier 10.1109/LRA.2022.3187504

A common approach for relative localization of vehicles is to adopt so-called fiducial markers. This approach involves the use of cameras and vision algorithms to estimate the position with respect to such fiducial markers which are usually binary square tags, such as the ArUco markers, placed on top of the vehicle to be followed [13], [14]. A wide experimental comparison reported in [15] proved that position estimation through fiducial markers has usually a mean error below 10 cm up to 2 m of distance from the marker itself at various angles.

However, the main limit of these solutions is that they can provide a localization outcome as long as the visual marker lies within the camera field of view. Moreover, medium to high computing resources are needed to perform the required computations, since usually high-resolution wide-fov cameras are needed.

Other indoor localization systems adopt triangulation-based solutions working with various technologies (e.g., ultra-wide band, bluetooth, ultrasound) or optitrack and VICON systems, which, however, require a structured environment, thus preventing the application of such systems whenever the intervention on the environment is unfeasible or when a prompt platform deployment is required.

Heterogeneous teams of tethered vehicles are scarcely investigated and often use the tethering system for data and power transmission only. Tether-based solutions for localization are rarely proposed in the literature, however, they can be profitably used also in so-called GPS-denied environments. The approach described in [8] adopts a commercial device [16] consisting of a drone and a base with a cable reel. The system performs the UAV control by measuring three values: 1) the length of the cable, 2) the angle between the tangent of the cable and a plane orthogonal to gravity (*elevation angle*), and 3) the angle of the cable with respect to the direction of the aerial vehicle (*azimuth angle*). These three measured values are used to derive the 3D position of the UAV with respect to the UGV in a polar reference system with an average error within 0.4 m in an indoor controlled environment. The two angles are measured at the attachment point of the cable to the aerial vehicle, while an encoder on the tether reel is used to measure the relative length of the unwound cable.

Another interesting approach is presented in [12] where the relative position of a multi-rotor with respect to an helipad placed on a construction machine is estimated. The helipad features a tether reel, designed in such a way to ensure the constant monitoring of the tension and length of the cable, as well as an ad hoc structure for the measurement of cable outlet direction. It is a custom device in which a clutch ensures a specified cable tension during the entire flight and low-friction potentiometers are attached to the cable outlet and the turntable to measure the pitch and yaw angles. The average error achieved with such an approach is about 1 m.

A recent work [17] proposes the adoption of an EKF-based recursive estimator to enhance the tether-based localization method for a slack tether with inertial data (namely tri-axial accelerations and angular velocities) acquired from the IMU onboard the UAV. The catenary equations are solved by measuring the cable length, tension, and the azimuth and elevation angles at both ends of the tether. The proposed approach has been validated in simulation and in a stationary real-world setting, achieving an average error within 50 cm with catenary equations only and within 20 cm by employing the EKF.

III. Proposed Solution

We propose a solution exploiting the detection of the cable angles at both ends of the tether, namely from both the anchor points on each vehicle. In [8] the proposed system is able to detect the position on a 2D vertical plane which is assumed to be fixed. In [12] the three measured quantities are used for tracking the UAV position in the space, whereas the attitude of the drone is neglected. Our proposed solution combines the strengths of the two approaches in order to increase the robustness of the position estimation without the need to sense cable tension as in [12] and [17], and allowing us to derive the heading difference between the vehicles.

A. Method

The main working hypothesis of tether-based localization solutions is that the tether connecting the two mobile robots assumes, under certain conditions, the geometrical configuration of a *catenary*. Under such a hypothesis, the well-known theory of a homogeneous suspended-line catenary can be exploited. In the following, we briefly recall some useful considerations to the scope of this work.

B. Catenary Arc

A flexible line charged only by its weight and suspended by two constraints at its ends, assumes in a vertical plane defined by $\vec{z}$ and $\vec{x}$ (respectively the upward vertical and the rightward horizontal unit vector) the so-called catenary configuration which is described by the following:

$$z = a\left(\cosh\frac{x}{a} - 1\right) \tag{1}$$

where a is a coefficient given by:

$$a = \frac{T_h}{\rho g} \tag{2}$$

Therefore, the configuration of the curve depends essentially on the coefficient a, which, in turn, depends on the linear density ρ of the cable and the horizontal component of the stress along the tether T_h. When no other external forces are applied to the line besides gravity, the stress horizontal component T_h along the catenary is constant throughout the cable. The hyperbolic curve described by (1) has a parabolic-like shape and its origin is taken at the vertex, i.e. at the intersection point of the catenary curve with its vertical axis of symmetry.

Any infinitesimal portion of the catenary is subject to the forces shown in Fig. 1. If T is the resultant stress of components (T_h, T_v) along the tether in the higher end and θ is the elevation angle still measured from the higher end:

$$\begin{cases} \sum F_x = 0 \Rightarrow T\cos\theta - T_h = 0 \\ \sum F_z = 0 \Rightarrow T\sin\theta - \rho g d L = 0 \end{cases} \tag{3}$$

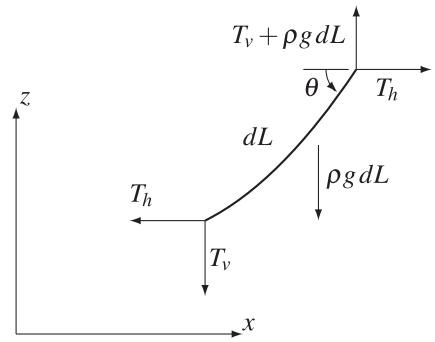

Fig. 1. Elementary length dL of the catenary.

Every geometric entity in the catenary can be expressed as a function of the elevation angle θ. Once the constant a is determined, the horizontal and vertical coordinates of a point along the catenary in the plane of the tether from the catenary origin are:

$$\begin{cases} x = sign(\theta) \cdot a \cdot \Psi(\theta) \\ z = a \cdot \left(\cosh \frac{x}{a} - 1 \right) \end{cases} \tag{4}$$

where for ease of notation we posed:

$$\Psi(\theta) = \ln \left(\tan \theta + \sqrt{\tan^2 \theta + 1} \right) \tag{5}$$

The arc length of the cable, from the origin of the catenary up to a point with coordinate x is given by:

$$S = a \cdot \sinh \frac{x}{a} \tag{6}$$

Since the origin is taken at the vertex of the catenary, S will be negative if the point lies on the left-hand branch of the catenary curve (i.e. $x < 0$), whereas it will be positive if the point lies on the right-hand branch of the catenary curve (i.e. $x > 0$).

C. Catenary Application to the Linking Tether

In the following, we will refer with G and A to the quantities related to the *ground* and the *aerial* vehicle respectively. It is worth noting that while the elevation angle on the UAV side θ_A is typically in the $(0, \pi/2)$ range (i.e. always positive), the elevation angle on the UGV side θ_G can be either positive or negative, roughly in the $(-\pi/2, \pi/2)$ interval.

Our estimation approach includes the case the two ends of the cable are in two different branches of the catenary as shown in Fig. 2 (i.e. $\theta_G < 0$). According to (6), the two arc lengths from the catenary origin up to the two ends are given by:

$$S_G = a \cdot \sinh \frac{x_G}{a} \quad \text{and} \quad S_A = a \cdot \sinh \frac{x_A}{a} \tag{7}$$

From which the full length of the tether can be derived:

$$L = S_A - S_G = a \cdot \left(\sinh \frac{x_A}{a} - \sinh \frac{x_G}{a} \right) \tag{8}$$

It is worth noting that if the tether ends lie on different catenary branches (as in Fig. 2) we have that $S_A > 0$ and $S_G < 0$ and (8) is actually a sum, whereas if the ends lie on the same branch, we have $S_A > S_G > 0$, hence $L > 0$. By substituting (4) in (8) and recalling that hyperbolic sine is an odd function, the constant a can be derived as:

$$a = \frac{L}{\sinh \Psi(\theta_A) - sign(\theta_G) \cdot \sinh \Psi(\theta_G)} \tag{9}$$

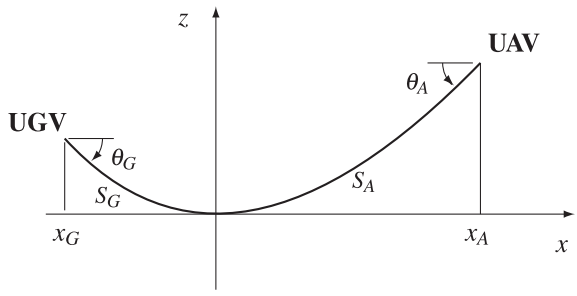

Fig. 2. Catenary configuration of the tether linking the aerial and the ground vehicles.

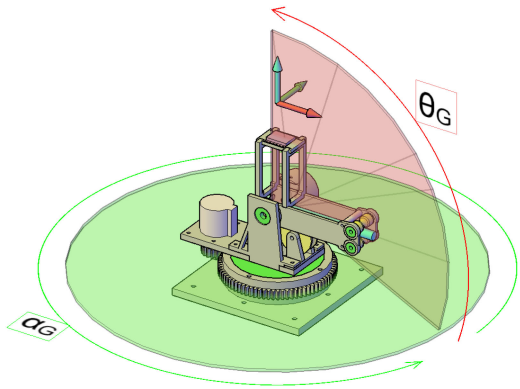

Fig. 3. Prototype of the sensor mounted on the UGV.

IV. Experimental Setup

A. Cable Direction Sensors

Two custom sensors have been mechanically designed and their prototypes realized through 3D printing in order to detect the direction of the cable at the lower and the higher ends, respectively on the UGV and on the UAV. We will refer to the former as *drift sensor* (Fig. 3), and to the latter as *gimbal sensor* (Fig. 4). Inspired by the work of Kiribayashi *et al.* [12], the sensor shown in Fig. 3 was developed. The structure has two potentiometers to sense the azimuth and elevation angles.

The UAV is equipped with the gimbal sensor which is used to measure the two angles shown in Fig. 5 through two rotary potentiometers. The developed prototype allows us to measure the cable angles in both directions without affecting the attitude of the UAV during the flight. From such measured angles the elevation (θ_A) and azimuth (α_A) angles are derived through a post-processing algorithm. The sensor, based on a gimbal-like structure with two degrees of freedom, has been designed and realized as a double concentric fork that ensures a smooth movement. Both the forks are linked to the previous structure level by means of ball bearings, in order to avoid mechanical

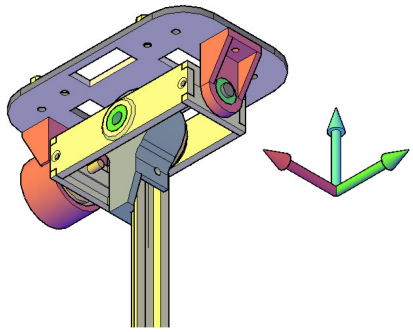

Fig. 4. Prototype of the sensor mounted under the UAV.

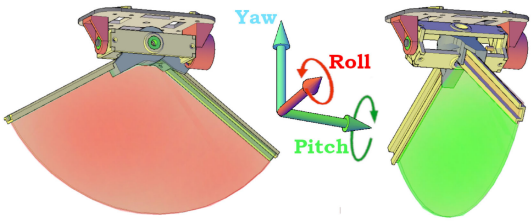

Fig. 5. Roll and pitch gimbal movements.

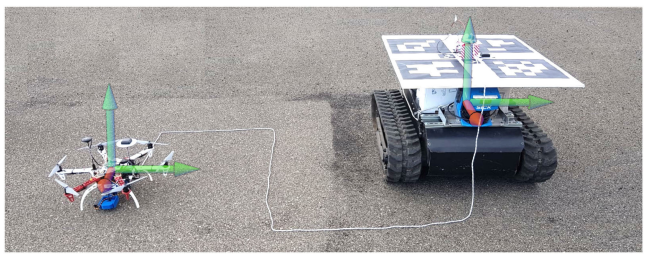

Fig. 6. The multi-robot tethered system.

Fig. 7. The multi-robot tethered system with the cable in catenary configuration during operation.

stress on the potentiometers shafts and measurement distortions. As can be seen in Fig. 4, a short shaft is used to link the cable to the sensor itself. This solution allowed us to sense better small angles of the cable end, compared to a single attachment point, as we experienced during the preliminary tests.

B. Multi-Robot System

The experimental robotic system used for this work is shown in Figs. 6 and 7. The former shows also the reference frames for each vehicle composing the multi-robot system.

The UAV adopted is a hexacopter, the DJI F550. A Pixhawk autopilot running the Ardupilot navigation stack is combined with an RTK GPS for centimetric accuracy in localization that we will use as a reference for data validation in the outdoor tests. The high-level control of the vehicle is managed by a companion computer, a Raspberry Pi3 B+. The UGV chosen is a tracked vehicle previously adopted for agricultural applications [18].

Our localization approach has been validated using a non-conductive fixed-length cable that replicates commercial products in terms of weight and cross-section. The length of the tether has always been kept within 5 m, since a much longer cable could not shape as a planar 2D catenary curve, due to vehicles' relative motion or wind, and, furthermore, may induce undesired jerks on the aerial vehicle due to the cable's inertia. The communication between the vehicles and an external ground control station is carried out on a dedicated 2.4 GHz Wi-Fi network.

C. Sensing Setups

The estimation of the position and, whenever possible, of the heading has been made with different sensor arrangements in order to determine the most robust and accurate solution.

1) Gimbal Sensor Only: In this setup the UAV is equipped with the sensor shown in Fig. 4, in order to derive the elevation (θ_A) and the azimuth (α_A) angles. Such a setup is conceptually equivalent to the approach proposed in [8]. Under the assumption that the cable elevation from the UGV (θ_G) is constant and equal to zero, it is possible to derive a from cable length and elevation from the UAV (θ_A) according to (9), while x_A and z_A are calculated according to (4). In this case the translation between UAV and UGV frames is:

$$\begin{cases} x = x_A \cos \alpha_G \\ y = x_A \sin \alpha_G \\ z = z_A \\ \alpha_G = \pi - \alpha_A - (h_G - h_A) \end{cases} \tag{10}$$

where h_G and h_A are respectively the UGV and the UAV headings acquired by the onboard IMUs.

2) Both Gimbal and Drift Sensor: The assumption of the UGV to be always in the origin of the catenary is often a rough approximation that introduces a non-negligible error. By including the drift sensor on board of the UGV the elevation and the azimuth angles can be measured from both the UGV and the UAV (θ_G, α_G, θ_A, α_A). Determining a with (4) it is possible to calculate x_A, z_A as before, but also z_G and x_G, which can be either positive or negative, depending on the sign of θ_G. In this case the relative position of the UAV frame w.r.t. to the UAV frame is given by:

$$\begin{cases} x &= (x_A - x_G)\cos\alpha_G \\ y &= (x_A - x_G)\sin\alpha_G \\ z &= z_A - z_G \\ \Theta &= \alpha_G + \alpha_A \end{cases} \tag{11}$$

It is worth noting that in this case it is possible to estimate the relative yaw direction (Θ), however, there is no possibility to estimate the full vehicle orientation.

3) Reference Data: A global shutter RGB camera acquiring 640×480 images at 30 fps is mounted under the UAV for marker detection through a 2D gimbal stabilizer, that allows the control of the camera orientation w.r.t. the vehicle frame. The camera is equipped with a lens with a focal length of 6.0 mm and a field of view of $35° \times 49°$ (vertical and horizontal respectively).

A 0.8×0.8 m ArUco board, printed on a platform mounted on top of the UGV, is used for the estimation of the relative position and orientation between the two vehicles, which has been used for comparison during the preliminary indoor tests after a careful camera calibration.

On the other hand, results obtained during the outdoor tests have been compared with the high-accuracy outcome of the extended Kalman filter for the UAV pose estimation [19] provided by the Ardupilot stack. As already mentioned, the data acquired by the onboard GPS receiver, enhanced with RTK differential corrections, allowed us to obtain a centimetric level accuracy.

V. Experimental Results

A. Indoor Static Tests

A preliminary indoor validation has been performed in order to assess the accuracy of the proposed localization with the two setups described in Section IV-C. These results are to be considered as an upper bound of the expected performance in the outdoor case, since the UAV is statically kept at well-measured predefined positions, thus removing any external source of disturbance and uncertainty due to wind and/or cable oscillations due to the relative motion of the vehicles, which may result in wrong tether angles readings from the potentiometers.

More in detail, seven positions evenly distributed along a semi-circle surrounding the ArUco marker (i.e. the UGV) have been chosen in order to have the cable in catenary configuration (i.e. not taut) and to test the sensing system at various elevation and azimuth angles. The tests have been performed with the aerial vehicle at an altitude 1.65 m (Fig. 8) and 2.22 m (Fig. 9) with respect to the marker and with the camera tilted to the left through the actuated gimbal with a roll angle of 45° to frame the marker. In this case the tether length was fixed at 3 m.

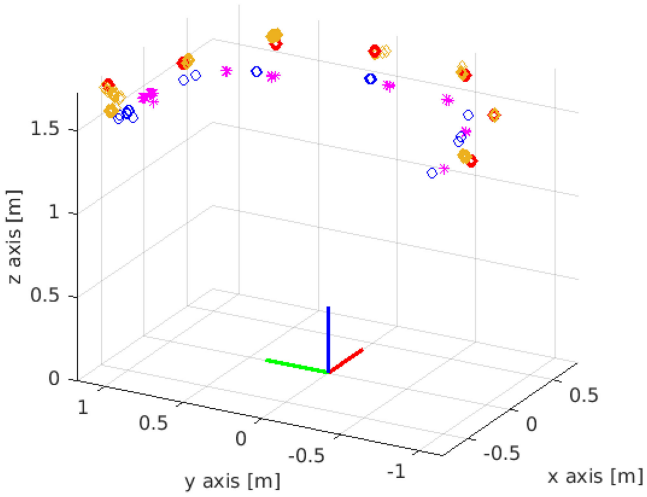

Fig. 8. Indoor static test results at 1.65 m: ground truth (red diamonds), ArUco (orange diamonds), gimbal sensor (blue circles), gimbal+drift sensor (magenta stars).

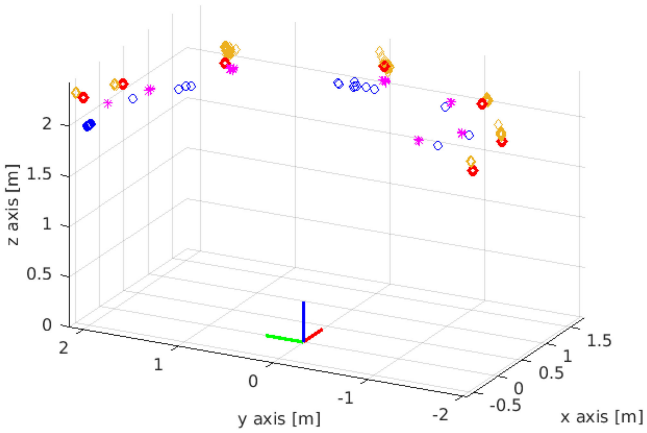

Fig. 9. Indoor static test results at 2.22 m: ground truth (red diamonds), ArUco (orange diamonds), gimbal sensor (blue circles), gimbal+drift sensor (magenta stars).

For each spot we acquired the position estimated with the two setups described in Section IV-C, i.e. with data from the gimbal sensor only and with sensors on both the vehicles, as well as the position estimated with the ArUco marker. For each position around 100 samples of data from each localization estimation method have been acquired in order to perform a statistical analysis on the results, namely the mean, the maximum, and the minimum Euclidean distance (i.e. the error between the recorded data and the ground truth positions). Table I reports the results of the statistical analysis.

As can be seen in Figs. 8 and 9, for each spot the positions estimated with our setups are essentially condensed around a point, even though such a point may fall at a certain distance from the ground truth. In fact, once the cable reaches the catenary equilibrium state and the vehicle is static, the position prediction according to sensors described in Section IV-C are essentially fixed as the potentiometer readings are stable. This can be quantitatively observed in Table I where, although minimum

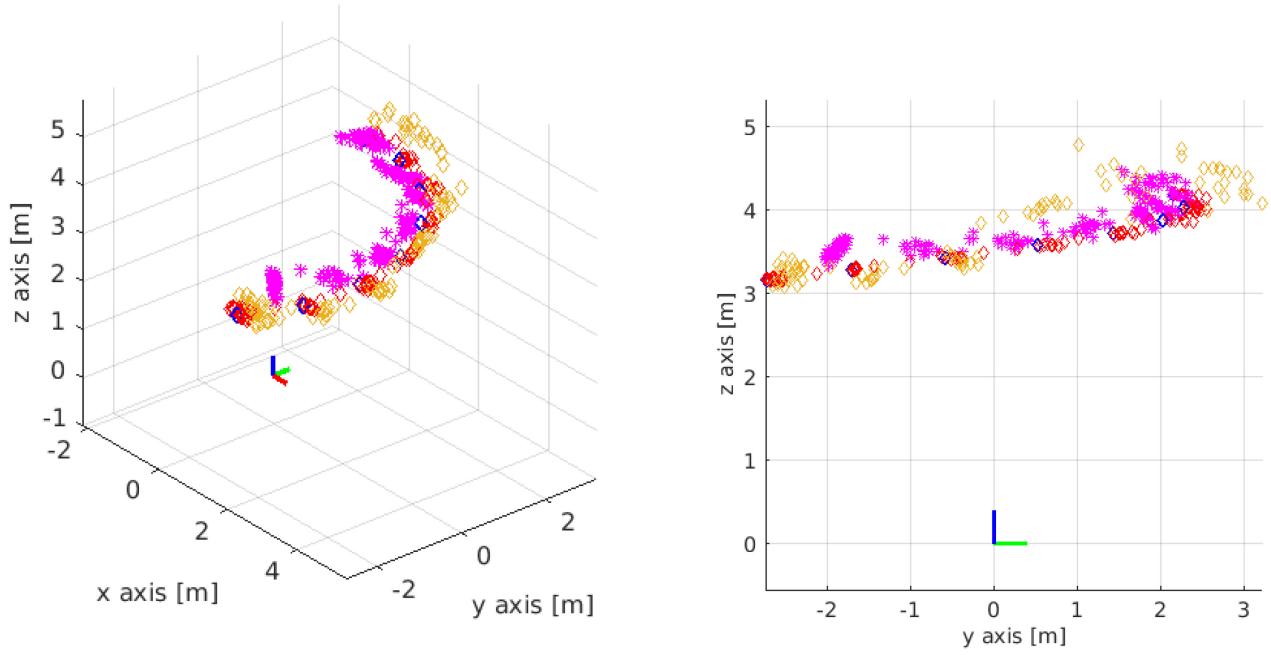

(a) Perspective view

(b) Front view

Fig. 10. Outdoor dynamic test results with the autonomous 8-waypoint mission: waypoints (blue diamonds), ground truth (red diamonds), ArUco (orange diamonds), gimbal+drift sensor (magenta stars).

TABLE I
STATISTICS ON THE RESULTS OBTAINED IN THE INDOOR STATIC TESTS

Height 1.65 m	**Mean [m]**	**Min [m]**	**Max [m]**	**Var [m^2]**
ArUco	0.0667	0.0082	0.4803	0.0091
Gimbal	0.2654	0.1759	0.3935	0.0046
Gimbal+drift	0.2185	0.1726	0.3576	0.0018
Height 2.22 m	**Mean [m]**	**Min [m]**	**Max [m]**	**Var [m^2]**
ArUco	0.0992	0.0274	0.1951	0.00065
Gimbal	0.3758	0.2383	0.5526	0.0099
Gimbal+drift	0.3331	0.2221	0.5972	0.0136

and average errors achieved with the ArUco are smaller than those obtained with our setups, the variances obtained with the latter are comparable or even smaller than the variance obtained with the ArUco.

B. Outdoor Tests

In light of the poor results obtained with the gimbal sensor only in the indoor experiments, we performed the outdoor tests with the full sensing setup (i.e. gimbal and drift sensors combined), as we expected we had to be robust to external disturbances, especially wind and oscillations induced by the vehicles' relative motion, which are much more relevant in the outdoor dynamic scenario.

The experimental trial has been conceived as an autonomous mission performed by the UAV surrounding the ground vehicle. The waypoints of the mission have been derived by fixing the cable length at 5 m and computing 8 points with the expected catenary formula (taking into account cable's linear density as well) with different values of elevation and azimuth angles. The resulting mission is an helicoid-like mission. It is worth to mention that the experimental mission has been designed also taking into account the camera field of view and the camera tilt so as to ensure that the outcome of the vision-based localization was always available for data comparison. Furthermore, we also equipped the camera with a neutral density filter to avoid overexposure. All the details of the outdoor dynamic test can be found in the video at the following link: https://youtu.be/cqG9-Qdp9_4.

Concerning the tether-based localization, only raw data from the method presented in Section III-A are shown both in the video and in Fig. 10. No filters are applied for smoothing data out or deleting outliers. This implies the possibility to further enhance the prediction outcome by including for instance a Kalman filter similarly to [17]. In the video it is also possible to appreciate the accurate heading prediction with the proposed solution combining the two sensors on board the two vehicles.

Surprisingly, the method proved to be stable even in presence of oscillations in the sensing of cable angles, which cause the temporary missed catenary configuration of the tether and the failing in the equilibrium state assumption. The tether-based estimation ensured appreciable results throughout the whole mission. We report the mean, the maximum, and the minimum Euclidean distance, i.e. the error, between each point logged during the trial and the related RTK-based logged point. Furthermore, the variance of the error array is performed. Since output data provided by each method were essentially asynchronous, particular attention has been paid to their proper synchronization for the comparison according to their timestamps. The obtained results are summarized in the upper part of Table II. The very large maximum error observed for the ArUco-based localization is due to a temporary missed marker detection, which is still proof of the limits of vision-based solutions.

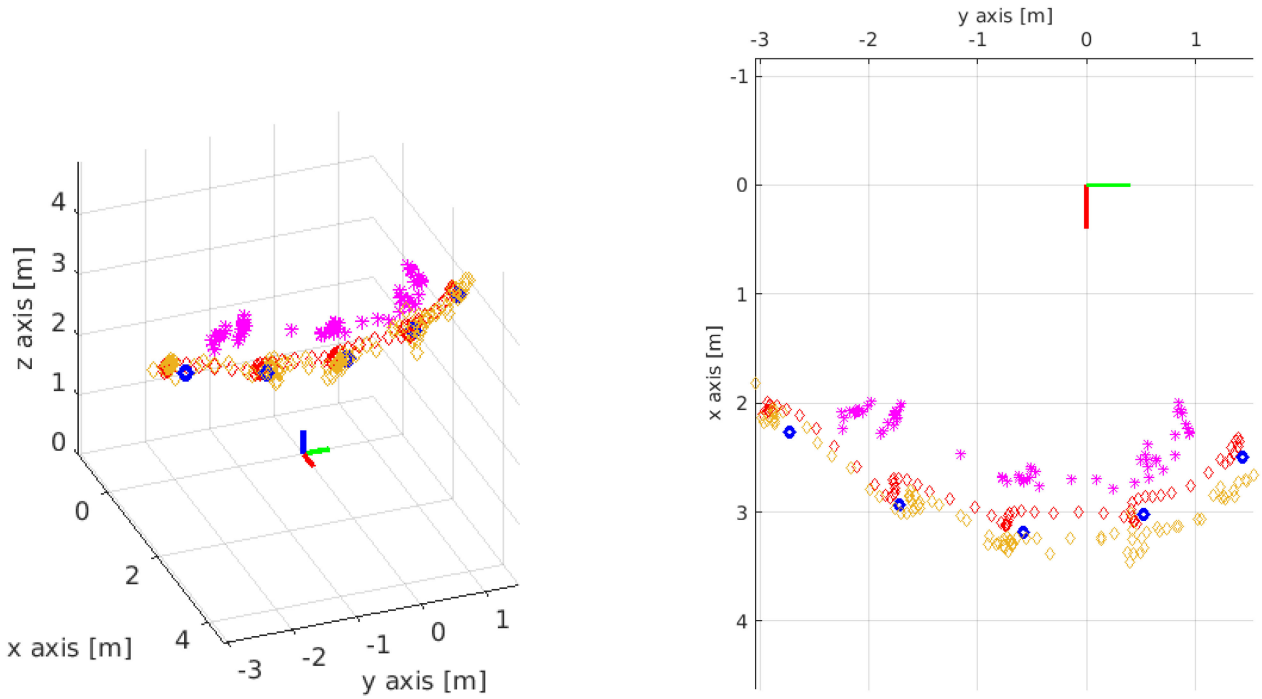

(a) Perspective view

(b) Top view

Fig. 11. Outdoor dynamic test results with the autonomous 5-waypoint mission: waypoints (blue diamonds), ground truth (red diamonds), ArUco (orange diamonds), gimbal+drift sensor (magenta stars).

TABLE II
STATISTICS ON THE RESULTS OBTAINED IN THE OUTDOOR TESTS

8-waypoint test	**Mean [m]**	**Min [m]**	**Max [m]**	**Var [m^2]**
ArUco	0.6110	0.0970	2.2482	0.1538
Gimbal+drift	0.7295	0.1566	1.2652	0.0462
5-waypoint test	**Mean [m]**	**Min [m]**	**Max [m]**	**Var [m^2]**
ArUco	0.2768	0.0492	0.6973	0.0158
Gimbal+drift	0.5988	0.2671	0.9670	0.0285

TABLE III
COMPARISON OF MEAN ERRORS ACHIEVED WITH OTHER TETHER-BASED METHODS

	[8]	**[12]**	**[17]**	**Ours**
Mean [m]	0.3675	1.046	0.4967	0.47
Tether length [m]	4	5	$\sim 3 \div \sim 4$	3 - 5

The results related to another experimental mission with 5 waypoints are shown in Fig. 11. In this case a more truthful comparison can be made since the ArUco localization did not experience any issue with the marker detection, whereas our solution performed slightly poorly between the first and the second waypoint, mainly due to some mechanical friction that limited the drift sensor rotation on the azimuth angle. This resulted in the large maximum error reported in the lower part of Table II. Table III reports a comparison between the mean errors achieved with the solutions described in Section II and ours (obtained as an average among the whole experimental trials).

VI. CONCLUSION

We presented a localization method for a pair of tethered vehicles, namely a field robot and a multi-rotor, leveraging the catenary shape of the cable. As opposed to the approaches typically adopted in the literature for GPS-denied environments, our solution allowed us to obtain an accuracy of around 0.22 m without the need to employ high-computing boards. We also achieved better results compared to the few examples of tether-based solutions available in the literature.

The encouraging results obtained in the outdoor dynamic tests, even in presence of several external disturbances and without any type of post-processing, suggest the possibility to profitably exploit the proposed localization solution as a further source for position estimation, even beyond the more intuitive indoor or GPS-denied application scenarios.

REFERENCES

[1] M. Petrlík, T. Báča, D. Heřčt, M. Vrba, T. Krajník, and M. Saska, "A robust UAV system for operations in a constrained environment," *IEEE Robot. Automat. Lett.*, vol. 5, no. 2, pp. 2169–2176, Apr. 2020.

[2] E. T. Alotaibi, S. S. Alqefari, and A. Koubaa, "LSAR: Multi-UAV collaboration for search and rescue missions," *IEEE Access*, vol. 7, pp. 55817–55832, 2019.

[3] M. Rahnemoonfar, T. Chowdhury, A. Sarkar, D. Varshney, M. Yari, and R. R. Murphy, "FloodNet: A high resolution aerial imagery dataset for post flood scene understanding," *IEEE Access*, vol. 9, pp. 89644–89654, 2021.

[4] M. M. Marques et al., "Chemical and radiological detection using UAV's with ATEX compliance: Proof of concept in port and maritime incident-based scenarios," in *Proc. IEEE OCEANS MTS Charleston*, 2018, pp. 1–5.
[5] A. Rabajczyk, J. Zboina, M. Zielecka, and R. Fellner, "Monitoring of selected CBRN threats in the air in industrial areas with the use of unmanned aerial vehicles," *Atmosphere*, vol. 11, no. 12, 2020, Art. no. 1373.
[6] D. A. Rico, F. Muñoz-Arriola, and C. Detweiler, "Trajectory selection for power-over-tether atmospheric sensing UAS," in *Proc. IEEE/RSJ Int. Conf. Intell. Robots Syst.*, 2021, pp. 2321–2328.
[7] K.-H. Chang and S.-K. Hung, "Design and implementation of a tether-powered hexacopter for long endurance missions," *Appl. Sci.*, vol. 11, no. 24, 2021, Art. no. 11887. [Online]. Available: https://www.mdpi.com/2076-3417/11/24/11887
[8] X. Xiao, Y. Fan, J. Dufek, and R. Murphy, "Indoor UAV localization using a tether," in *Proc. IEEE Int. Symp. Saf. Secur. Rescue Robot.*, 2018, pp. 1–6.
[9] X. Xiao, J. Dufek, and R. R. Murphy, "Autonomous visual assistance for robot operations using a tethered UAV," in *Field and Service Robotics*, G. Ishigami and K. Yoshida, Eds. Singapore: Springer, 2021, pp. 15–29.
[10] G. Sutera, A. Borgese, D. C. Guastella, L. Cantelli, and G. Muscato, "A multi-robot system for thermal vision inspection," in *Proc. 23rd Int. Symp. Meas. Control Robot.*, 2020, pp. 1–6.
[11] K. A. Talke, M. De Oliveira, and T. Bewley, "Catenary tether shape analysis for a UAV - USV team," in *Proc. IEEE/RSJ Int. Conf. Intell. Robots Syst.*, 2018, pp. 7803–7809.
[12] S. Kiribayashi, K. Yakushigawa, and K. Nagatani, "Position estimation of tethered micro unmanned aerial vehicle by observing the slack tether," in *Proc. IEEE Int. Symp. Saf. Secur. Rescue Robot.*, 2017, pp. 159–165.
[13] A. Marut, K. Wojtowicz, and K. Falkowski, "ArUco markers pose estimation in UAV landing aid system," in *Proc. IEEE 5th Int. Workshop Metrol. Aerosp.*, 2019, pp. 261–266.
[14] S. M. Nogar, "Autonomous landing of a UAV on a moving ground vehicle in a GPS denied environment," in *Proc. IEEE Int. Symp. Saf. Secur. Rescue Robot.*, 2020, pp. 77–83.
[15] M. Kalaitzakis, S. Carroll, A. Ambrosi, C. Whitehead, and N. Vitzilaios, "Experimental comparison of fiducial markers for pose estimation," in *Proc. Int. Conf. Unmanned Aircr. Syst.*, 2020, pp. 781–789.
[16] Fotokite website. Feb. 2022. [Online]. Available: https://fotokite.com/
[17] R. R. Lima and G. A. S. Pereira, "On the development of a tether-based drone localization system," in *Proc. Int. Conf. Unmanned Aircr. Syst.*, 2021, pp. 195–201.
[18] L. Cantelli, F. Bonaccorso, D. Longo, G. Schillaci, C. D. Melita, and G. Muscato, "A small versatile electrical robot for autonomous spraying in agriculture," *AgriEngineering*, vol. 1, no. 3, pp. 391–402, Aug. 2019.
[19] Ardupilot extended Kalman filter. Feb. 2022. [Online]. Available: https://ardupilot.org/dev/docs/extended-kalman-filter.html#extended-kalman-filter